Kovove Mater. 48 2010 105–115
DOI: 10.4149/km_2010_2_105

Role of plasma nitriding temperature and time in the corrosion behaviour and microstructure evolution of 15-5 PH stainless steel

E. A. Bernardelli[1], P. C. Borges[1*] , L. C. Fontana[2], J. B. Floriano[1]

[1]*Federal Technological University of the Paraná, UTFPR, DAMEC, 80230-901, Curitiba-PR, Brazil*
[2]*State University of Santa Catarina UDESC/Joinville, Brazil*

Received 29 May 2009, received in revised form 22 October 2009, accepted 26 November 2009

Abstract

Simultaneous plasma nitriding and ageing were performed on 15-5 PH stainless steel, being the treatment time (2, 4 and 6 h) and temperature (390, 440 and 490 °C) the control variables. The highest value for core hardness was obtained at the longest time (6 h) and the lowest temperature (390 °C). A long treatment time (6 h) and high temperature (490 °C) have favoured the surface layer formation. The formation of expanded martensite α_N and expanded austenite γ_N was observed using low nitriding temperature, while raising the temperature favoured the formation of the γ' and CrN phases. When the treatment was carried out at temperatures of 440 and 490 °C, a drop in the corrosion resistance was observed. Treatment at 390 °C led to an improvement in the corrosion potential ($E_{I=0}$), however, the samples processed at 390 °C did not show a clear passive region.

K e y w o r d s: plasma nitriding, ageing, 15-5 PH stainless steel, phase formation, corrosion

1. Introduction

Martensitic and precipitation hardening stainless steels are recommended for applications where a combination of mechanical strength and corrosion resistance are required. In addition to chromium as the main alloying element, precipitation-hardening stainless steels contain copper as substitution alloying element, which increases the mechanical resistance by precipitation hardening. The ageing treatment is generally carried out at 450–620 °C, for a given time. Although precipitation-hardening stainless steel is characterized by high bulk hardness as compared to, say, austenitic stainless steel, it is desirable to improve the surface properties with respect to wear and corrosion resistance [1]. The relatively high bulk hardness combined with a hard and wear resistant surface layer would expand the application range. Traditionally, thermochemical processes, e.g. plasma nitriding treatment, improve the strength and wear resistance of this steel [2–4].

The nitriding of stainless steels may lead to precipitation of CrN in the surface layer, with consequent reduction on the corrosion resistance. Recent studies have shown that if stainless steels are nitrided at temperatures below 450 °C, diffusion of chromium is reduced and the formation of chromium-rich precipitates is inhibited, thus improving the corrosion resistance [5, 6]. However, Oddershede et al. [7] have nitrided 316 austenitic stainless steel and observed that at low temperature (445 °C) there occurred the formation of CrN precipitates.

Results published by Menthe et al. [8] for nitrided 304L stainless steel at 450 °C point out that the resistance to localized corrosion increased in the presence of a 2 % NaCl solution. In a study of the nitriding process in 17-4 PH stainless steel at temperatures of 400, 450, 480 and 500 °C, Marinho et al. [9] found that the corrosion resistance, using a 3 % NaCl solution, increased for all the conditions studied, however, the corrosion current density was greater than in the supersaturated state.

Mändl et al. [10] have investigated the treatment of stainless steel AISI 630 using low energy nitrogen implantation and high nitrogen plasma immersion ion implantation (PIII). They concluded that it can be stated that high energy implantation at 380 °C leads to lattice expansion with few contaminations of

*Corresponding author: tel.: +55 41 3310-4783; fax: +55 41 3310-4660; e-mail address: pborges@utfpr.edu.br

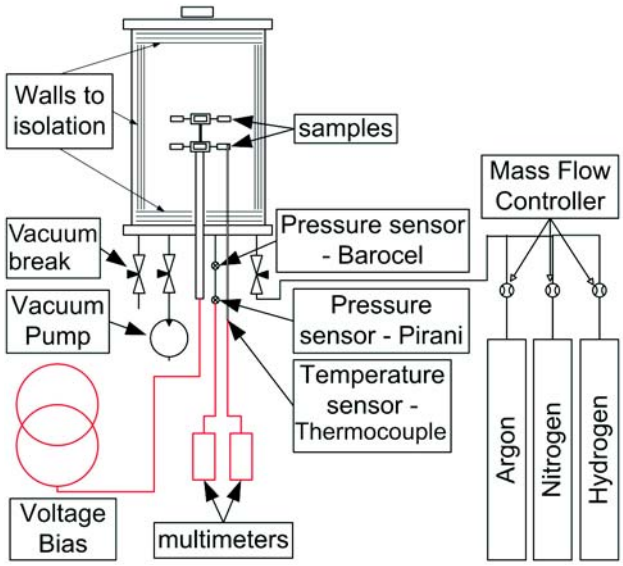

Fig. 1. The plasma reactor utilized on nitriding and ageing experiments.

Fe_3N, whereas low energy implantation leads to Fe_4N phase formation at low temperatures and CrN precipitates at high temperatures (600 °C). Thus, two different hardening mechanisms – formation of a hard phase and precipitation hardening – are observed, depending on the implantation conditions. Using low temperature treatment (380 °C) the corrosion resistance should remain the same because there is still free Cr available to form an oxide layer. When the treatment was realized at 600 °C the Cr was removed in the form of CrN precipitates reducing the corrosion resistance.

Lei et al. [11] worked with nitridation of 18-8 austenitic stainless steel at 280 °C and found that the martensite (α'_N) could form from the nitrogen-containing disordered fcc phase. During the process the α'_N martensite later transformed to the disordered nitrogen-containing hcp phase (α_N). The result is that, when the surface possesses $\alpha'_N + \gamma_N$ mixed phase or γ_N, no pitting corrosion occurs. It is shown that the α'_N martensite formation in the γ_N phase matrix did not affect the pitting corrosion resistance of the nitride stainless steel. The breakdown protection potentials for the $\alpha_N + \gamma_N$ mixed phase were lower than those of the $\alpha'_N + \gamma_N$ mixed phase. The α_N phase transformation from the α'_N martensite led to severe deterioration of pitting corrosion resistance of the nitrided stainless steel. However, the pitting corrosion resistance of $\varepsilon_N + \gamma_N$ mixed phase was similar to that of the original stainless steel.

Esfandiari et al. [12] investigated the temperature and time of plasma nitriding of 17-4 PH martensitic and A286 austenitic stainless steel. They concluded that a considerable improvement in wear resistance was possible without compromising corrosion resistance properties. They investigated the corrosion resistance by anodic polarization method in a 3.5 % NaCl solution of the untreated and as-nitrided samples. They attributed a significant increase in pitting corrosion resistance to the formation of a uniform γ'-Fe_4N layer on the surface of samples treated at 420 °C for 10 h. However, samples treated at high temperature (500 °C) revealed very poor corrosion behaviour, due to the formation of chromium nitrides (CrN).

The effect of nitriding on the microstructure of precipitation-hardened steels has recently been the focus of studies by various authors [1, 12–14]. Gui-Jiang Li [2] has studied the wear resistance as well as microstructure evolution. However, there are very few studies, which address the 15-5 PH stainless steel.

The aim of this study was to determine the influence of temperature and duration of plasma nitriding when carried out at the same time as ageing, on corrosion resistance and microstructural evolution of the 15-5 PH stainless steel.

2. Experimental

The samples were prepared from grade 15-5 PH stainless steel with the following composition (wt.%): 0.046 C; 0.42 Si; 0.71 Mn; 0.021 P; 0.012 S; 14.35 Cr; 4.78 Ni; 3.31 Cu; 0.3 Mo; 0.058 V with Fe in balance.

Solution treatment was carried out at 1175 °C for two hours, followed by cooling in water at ambient temperature (25 °C). The supersaturated samples were identified as S1175. The treatment was carried out in a salt bath with automatic temperature control.

After the supersaturating treatment, the samples were cut into 15 × 15 × 7 mm^3 sections, prepared metallographically by polishing with 1 μm diamond suspension and then immersed in alcohol and cleaned in an ultrasonic bath.

The nitriding and ageing experiments were conducted on a reactor plasma (Fig. 1) with DC tension source with pulse width modulation control, being possible to obtain different working temperature changing the time on and time off. The wall of the reactor is the anode, with three walls of stainless steel to minimize the thermal gradient, and the samples are positioned radial in the centre. The samples were positioned directly on the cathode and heated only by ionic bombardment, being that the temperature was measured directly in two samples by type K thermocouple. The identification assigned to each sample and the respective processing conditions is shown in Table 1. This reactor was similar to reactor used in Borges [15].

Before nitriding, the material was pre-cleaned by plasma (Table 1). It was realized to remove the oxides from the surface, improving the efficiency of the nitriding process [3, 16, 17].

Table 1. The nitriding conditions used in the study and the identification assigned to each sample

Parameters	Temp. (℃)	Time (h)	Identification	Pressure (torr)	Flow (sccm)	Gas mixture (%)	Voltage (V)
Cleanness by plasma	150	0.5	–	1.5	100	100 H_2	400
Plasma nitriding treatment	390	2	$N390_2$	3	200	80 N_2/20 H_2	400
	390	6	$N390_6$				
	440	2	$N440_2$				
	440	4	$N440_4$				
	490	2	$N490_2$				
	490	6	$N490_6$				

After the samples had been nitrided, they were cut and prepared metallographically by polishing with a 1 μm diamond suspension and etching with reagent Marble (200 ml H_2O + 200 ml HCl + 40 g $CuSO_4$) for 3 seconds. The samples for analysis of cross sections after corrosion tests were cut by precision cut equipment model Miniton (from Struers) and embedded in an epoxy resin (DuroFast from Struers).

Microhardness measurements were performed using a Shimadzu HMV 2000 microhardness tester. Loads of 0.02 kg and 0.1 kg were used for the surface (top microhardness) and core, respectively. The load of 0.02 kg for the surface is performed to minimize the substrate effects in the microhardness value [4]. The microhardness values determined are the result from the average value of five indentations.

The microstructure was characterized using a Zeiss Neophot 32 optical microscope, and the thickness of the surface layer was measured using two samples, with five fields per sample and five measurements per field. The results for the microhardness and thickness of the surface layer were analysed using t-test Student.

The different phases formed were characterized by X-ray diffraction techniques. The diffraction parameters were as follows: Cu Kα radiation; angle range (2θ) of 30° to 90°, voltage 30 kV, current 40 mA, scan step size of 0.02°, and a scan step time of 1 s. The program utilized was Philips X'Pert version 1.2 A.

E_{corr}-versus-time and cyclic polarization tests were carried out in a three-electrode electrochemical cell in order to evaluate the corrosion resistance. The working electrode in the supersaturated state (S1175) was tested after the fine polishing using 1 μm diamond particle suspension. The nitrided and aged working electrode was tested as processed. A calomel electrode was used as reference electrode, and the potential values were plotted based on the NHE standard. The counter-electrode was carbon black.

The equipment utilized in the corrosion tests was the EG&G Princeton Applied Research (PARC) model 273 potentiostat/galvanostat, using a 0.5 mol L^{-1} NaCl solution. A scan rate of 0.166 mV s^{-1} was used in these tests, as recommended in ASTM G5-94. All the tests were carried out at 25℃. The corrosion results hereby presented were averaged from five tests for each condition studied.

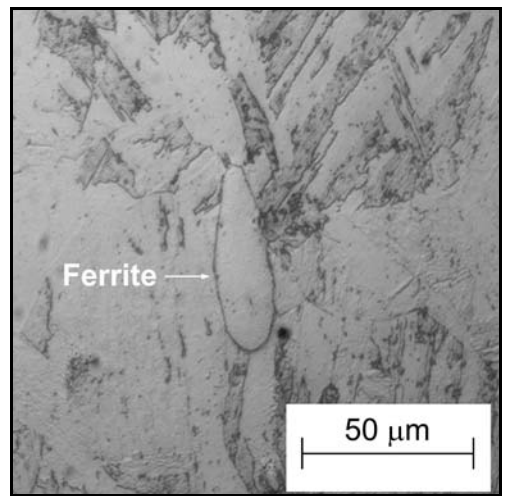

Fig. 2. Microstructure of sample S1175 (etched with Marble's reagent) viewed under an optical microscope.

3. Results and discussion

3.1. Simultaneous ageing and nitriding

The supersaturation treatment has proved to be effective, as the hardness of the steel dropped from its initial as-supplied value (402.1 ± 15.2) HV to (346.6 ± 6.7) HV.

Figure 2 shows the micrograph of the 15-5 PH steel in the supersaturated state (S1175). Metallographic examination revealed that the material had a microstructure composed of packets of martensite laths and the presence of ferrite could be observed, too. Microhardness measurements in the ferrite region have yielded a hardness of (269.4 ± 12.6) HV, when compared to the hardness value for the matrix, this phase hardness is by 77.2 HV lower.

Table 2. Core (h_c) and surface layer microhardness (h_l) and thickness (t_l) as a function of treatment time and temperature

Condition	h_c, HV	h_l, HV	t_l (μm)
$N390_2$	464.5 ± 9.1	1278.1 ± 78.5	5.5 ± 0.3
$N390_6$	488.4 ± 9.7	1295.6 ± 45.6	11.6 ± 1.5
$N440_2$	488.0 ± 5.5	1089.9 ± 66.0	11.2 ± 1.0
$N440_4$	473.3 ± 4.5	1318.5 ± 55.4	20.5 ± 1.2
$N490_2$	433.7 ± 8.3	1210.2 ± 76.4	27.7 ± 1.8
$N490_6$	428.7 ± 5.7	1779.2 ± 48.2	41.4 ± 2.6

The mean values of core hardness (h_c), layer thickness (t_l) and layer hardness (h_l) as a function of treatment time and temperature are given in Table 2.

It can be seen from Table 2 that the highest core hardness values were obtained for the conditions $N440_2$ and $N390_6$. According to Bajguirani [18] and Habibi [19], when ageing is carried out at these temperatures, the precipitates formed have 9R and 3R structures and are finely distributed in the matrix.

It is believed that the hardness value obtained for the conditions $N390_6$ is not the maximum viable hardness for this temperature, being that it is corroborated by the hardness value obtained for the conditions $N440_2$, which is statistically equal to the hardness value for the conditions $N390_6$. It is known that as the ageing temperature is raised, the peak hardness is reached faster; however, this value is lower than the hardness that can be achieved for treatments at lower temperature [20]. This allows us to conclude that, for the temperature conditions studied, the core hardness is favoured at lower temperature and at longer treatment time.

The conditions $N390_2$, $N440_2$ and $N490_2$ (Table 2) show that when the temperature increased from 390 to 440 °C, an increase in core hardness occurred. However, when the temperature increased from 440 to 490 °C the core hardness was reduced, indicating that for the conditions $N490_2$ the process of overageing had already started.

The overageing observed at 490 °C must be related to the evolution of the 3R structure into an FCC (face-centred cubic) structure, as described by Bajguirani [18] and Habibi [19]. Statistically, the core hardness of sample $N440_4$ is lower than that of $N440_2$ (Table 2). This small reduction in hardness leads us to believe that the sample $N440_4$ may already be in the overageing stage.

Surface layer thickness was found to increase concordantly with increasing treatment temperature for the conditions studied (Table 2). This layer would be expected to become thicker with rising temperature, with consequent increase in diffusion coefficient [21], particularly for the conditions analysed in this study, where the rise in temperature was achieved by increasing the frequency of the pulsed-current power supply, which favoured the formation of the surface layer, too [22].

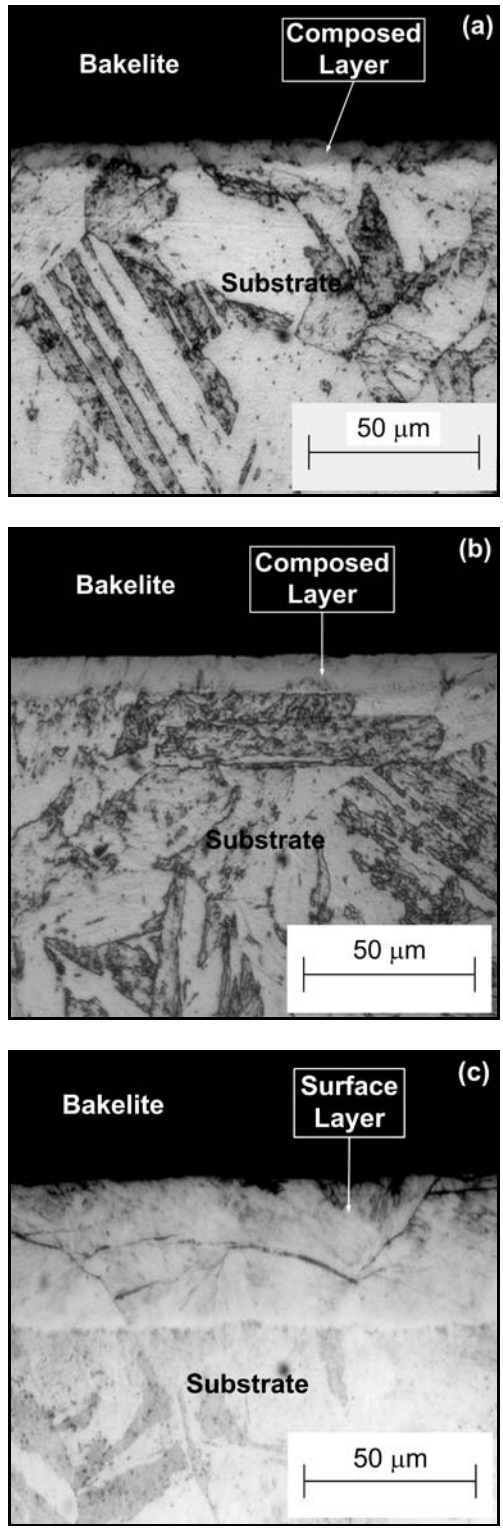

Fig. 3. Micrographs for nitrided conditions: a) $N390_2$, b) $N390_6$, c) $N490_6$.

It can also be seen in Table 2 that the increase in treatment temperature had a greater influence than time on the formation of the abovementioned surface layer. This is probably due to the reduction in the concentration gradient between the medium and the part, as well as a smaller diffusion coefficient in the surface layer than in the substrate (e.g., nitrogen diffusion coefficients ($cm^2\,s^{-1}$) at 500 °C: α phase = 3.624×10^{-8}; γ' phase = 7.985×10^{-9}; and ε phase = 1.017×10^{-10}) [21].

With regard to the surface layer hardness, the analysis of Table 2 reveals that it increases monotonically in time. This behaviour was not observed when the temperature changed, and the lowest values of hardness were found for nitriding at 440 °C. The effect of temperature on the hardness of the surface layers is discussed in section 3.2.

Figure 3 shows micrographs of the substrate and surface layer for the conditions $N390_2$, $N390_6$ and $N490_6$. It can be seen from these figures that the surface layer of the samples nitrided at 390 °C was resistant to chemical attack by reagent Marble [23]. At higher treatment temperatures, the transition between the substrate and the surface layer was more pronounced. It is evident that the compound layers and substrate have different corrosion rates, as wt.% of chromium in solutions is different in these regions.

At the treatment temperature of 490 °C (Fig. 3c), cracks have occurred in the surface layer. According to Frandsen et al. [14] and Yetim et al. [24], nitridation leads to a high level of residual stresses in the surface layer, and these cracks result from the relaxation that occurs during metallographic preparation. According to Jeong and Kim [22], these stresses were produced during the formation of the CrN and Fe_4N phases. Optical microscopy surface analysis of samples nitrided at 490 °C, before and after hardness indentations, did not reveal any cracks, which suggested that the existing cracks were indeed formed during metallographic preparation.

3.2. X-ray diffraction (XRD)

The X-ray diffraction patterns for the surface layer structures and phases are shown in Fig. 4. The XRD analysis shows the gradual changes in the constituents of the nitrided layer as the nitriding temperature and time increased.

The sharp peaks in Fig. 4a correspond to the martensite (α') phase peaks in the non-nitrided or supersaturated samples (S1175). Figure 4a shows the XRD patterns of thermally treated specimens, too. It can be seen that as the temperature increases, the peaks corresponding to the γ' and CrN phases increase, indicating that for the conditions studied, both the γ' and CrN phases are favoured at higher temperatures [24], whereas the intensity of the ε peaks decreases, which is in agreement with Sun et al. [23]. Oddershede et al. [7] have evidenced that the development of CrN retrieves Cr atoms from solid solution and effectively yields a matrix rich in Fe and Ni and, subsequently, the iron-based nitrides γ' and ε can develop in the matrix more easily.

It can also be seen (Fig. 4a) that at lower temperatures the peaks are broader and not well defined. Many factors besides the particle size are likely to contribute to the observed broadening as, for instance, composition and/or lattice strain variations, i.e. microstresses. It has been shown by Oddershede et al. [7] that the presence of deformation stacking faults and screw dislocations in expanded austenite has an influence on the line profiles. These results agree with those reported by Dong et al. and Li et al. [1, 6]; according to them, these phases are nitrogen-supersaturated martensite (α'_N) and expanded austenite (γ_N).

Initially, the matrix is α' martensite (see S1175 in Fig. 4a), and with the introduction of nitrogen the α' phase transforms into α'_N. Being nitrogen a stabilizer of austenite, the introduction of further nitrogen induces the formation of γ austenite (fcc). Consequently, at lower nitriding temperatures the α' grains are able to transform first to α'_N grains, and if more nitrogen is introduced, the α'_N phase is then transformed into the γ_N phase. Compared with the untreated samples, those nitrided at 390 °C have broader peaks, which correspond to the expanded martensite (α'_N) and expanded austenite (γ_N) phases. These results are in agreement with those reported by Frandsen et al. [14].

The diffraction patterns obtained for the samples S1175, $N440_2$ and $N440_4$ are shown in Fig. 4b. As the treatment time is extended, the intensity of the peaks corresponding to the γ' and CrN phases increases, while the intensity of the ε peaks decreases. The intensity of the diffraction peaks for the γ_N phase also increases slightly, and the peaks shift to higher 2θ angles. This indicates that at higher temperatures the γ_N phase had less nitrogen in solid solution and consequently, the interplanar space was smaller. Valencia-Alvarado et al. [25] also found that treatment conditions influenced supersaturation and consequently, the γ_N phase corresponding peak position.

It can be seen in Fig. 4c that, if treatment time is extended, the intensity of the peaks corresponding to the ε and α'_N phases decreases, while the peak for the γ'_N phase increases.

The analysis of the diffractograms in Fig. 4d allows us to conclude that, at 490 °C, increasing treatment time, from 2 to 6 h, has led to an increase in the intensity of the diffraction peaks corresponding to the α', γ' and CrN phases as well as to a reduction in the intensity of the remaining peaks; i.e., the γ' and CrN phases become more stable, suggesting that precipitation of the CrN phase causes nitrogen impoverishment in the neighbouring area. The loss of

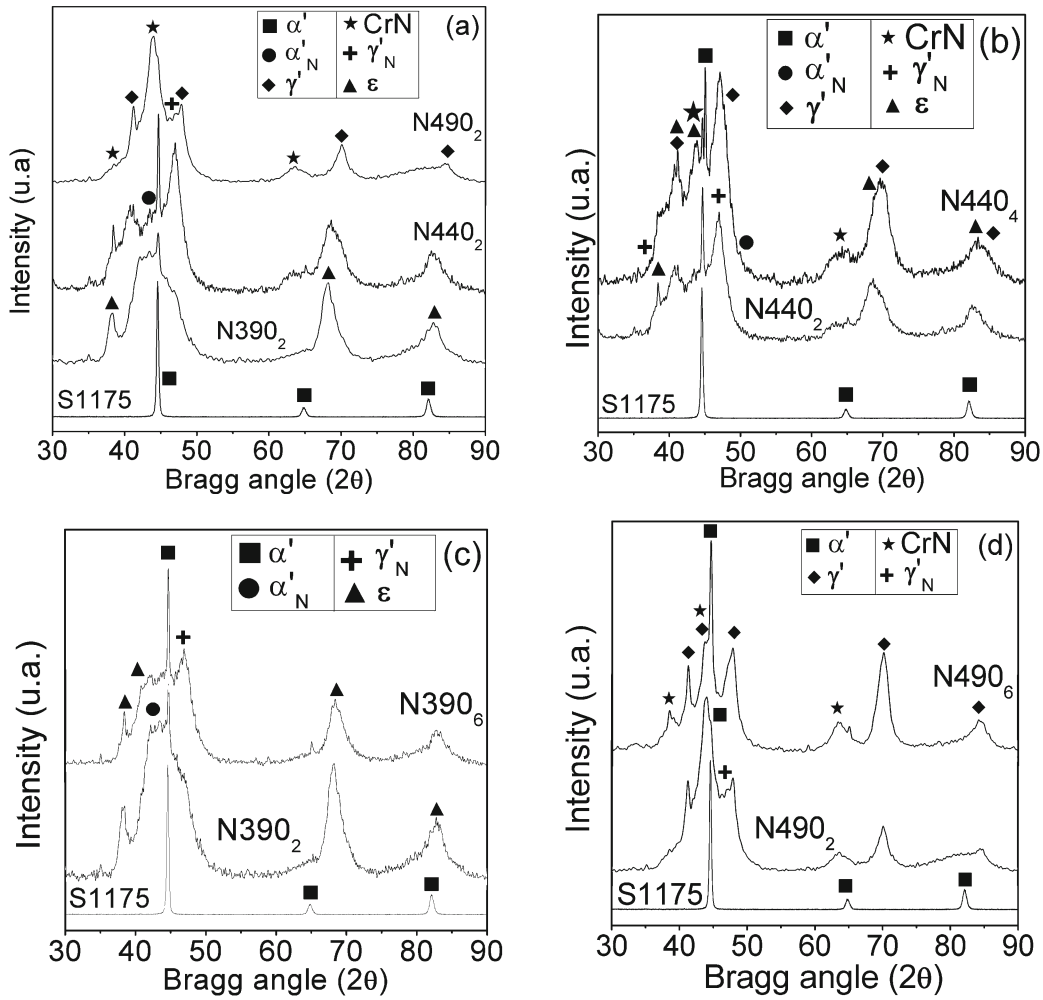

Fig. 4. X-ray diffractograms: a) S1175, $N390_2$, $N440_2$ and $N490_2$; b) S1175, $N440_2$ and $N440_4$; c) S1175, $N390_2$ and $N390_6$; d) S1175, $N490_2$ and $N490_6$.

nitrogen to the CrN phase suggests that those phases containing less nitrogen (e.g., the α' phase) appear in the neighbouring area. In other words, increasing the treatment time, the ε and γ_N phases become supersaturated with nitrogen and consequently convert as follows: $\varepsilon \rightarrow \mathrm{CrN} + \alpha'$ and $\gamma_N \rightarrow \gamma'$.

Correlating the results in Fig. 4a with the values obtained for the surface layer hardness in Table 2, it can be seen that minimum hardness is reached at a temperature of 440 °C for a treatment time of 2 h. XRD analysis shows that the surface layer hardness at this temperature is a function of the amount of α' phase. When the temperature rises from 390 to 440 °C (Fig. 4a), the α' peak intensity can be seen to increase in relation to those of the other ε and α_N peaks. This suggests that, at higher temperature, there are probably larger and smaller amounts of ε and α_N precipitates, respectively. There is also the contribution of the CrN precipitates, despite their high hardness; they are probably present in small amounts due to the relatively low temperature (440 °C). Consequently, the average distance between these precipitates would be larger at this temperature, thus decreasing the dispersion strengthening and consequently the reduction in hardness.

As the increase in temperature continues (from 440 to 490 °C), a change in this phenomenon can be observed: a large amount of γ' and CrN is formed, showed in the XRD diffractograms by the main peak coinciding with the CrN peak (200), that has lead to an increase in hardness, in accordance with Esfandiari and Dong [12]. The hardness increase, in this case, may be due to a reduction in the average distance between the precipitates, as well as to the higher hardness of the CrN precipitate now present in the surface layer (Figs. 4a,d).

It can be seen from the hardness values for treatment conditions $N440_2$ and $N440_4$ that extending the treatment time from 2 to 4 h has led to an increase in the hardness of the surface layer. The analysis of the X-ray diffraction spectra shows that the superficial hardness may have been influenced by the increase in

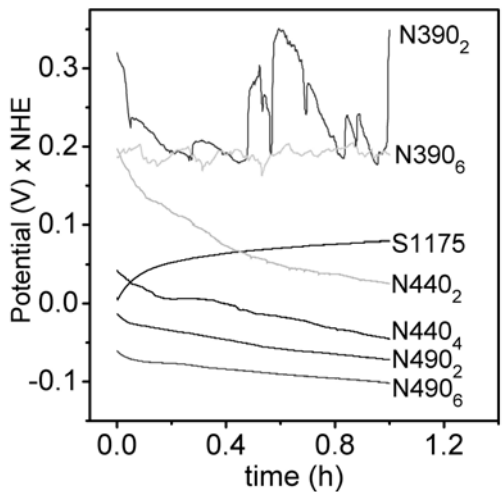

Fig. 5. Open circuit potential curve (E_{corr} *vs* time) for the treatment conditions studied.

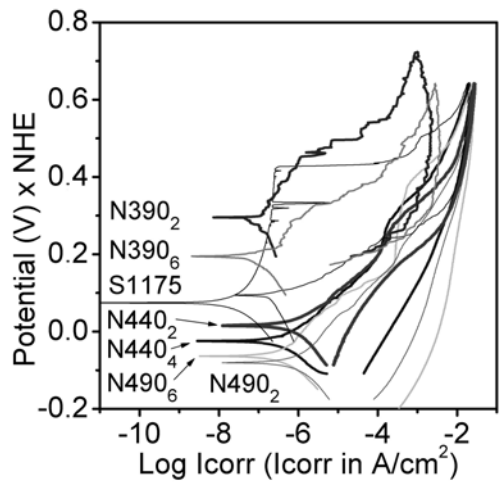

Fig. 6. Cyclic polarization curves for the treatment conditions studied.

the amount of CrN phase and γ' phase. Similar results were also observed for samples processed at 490 ℃.

No significant change was observed concerning the hardness of the surface layer in samples nitrided at low temperature (390 ℃) when the treatment time was extended from 2 to 6 h, there were not any significant changes in the amount of each phase formed.

3.3. Corrosion resistance

The corrosion tests were realized based on ASTM G5 [26]. The relationship between open circuit potential (OCP) and time is presented in Fig. 5. It can be seen that the supersaturated conditions S1175 raised the potential to nobler values, which indicates a clear tendency to passivation in the electrolytic medium studied.

While the conditions N390$_2$ and N390$_6$ (Fig. 5) have yielded nobler potentials than the other treatment conditions, wider variations in the potential were observed under these conditions to all samples. Although there is an indication of a tendency for film formation during open-circuit potential, this film is soluble in the utilized electrolytic medium. The results obtained for the conditions N440$_2$, N440$_4$, N490$_2$ and N490$_6$ have shown that the film dissolved accompanied by consequent reduction in potential.

Figure 6 shows the results for cyclic polarization. It can be seen that when nitriding was carried out at 390 ℃, the corrosion potential ($E_{I=0}$) was higher than the results obtained for the other treatment conditions. This is in agreement with [6, 24] where the results show that nitrogen enrichment has the effect to shift the potential to a nobler value. When the stainless steel rich in interstitial nitrogen atoms is submitted to corrosion process, the interstitial nitrogen atoms are released. These atoms can react with H^+ to form NH_3, consequently, the pH to this cathodic reaction increase allows to facilitate the repassivation [24]. Adding the nitrogen effect, at low temperature the diffusion of chromium is reduced and the formation of chromium-rich precipitates is difficult, thus improving corrosion resistance [5, 6, 24].

At low temperature, the formation of the martensite (α'_N) and expanded austenite (γ_N) (Fig. 4) in agreement with [11] can improve localized corrosion resistance. However, when the time of treatment is prolonged, the localized corrosion resistance could worsen as a result of the formation of α_N [11]. These results can be observed in Fig. 6, where the samples nitrided for 2 h at 390 ℃ showed higher corrosion resistance than those nitrided for 6 h at 390 ℃. Discussions regarding the effect of the phase types in the corrosion resistance are still ongoing, for the issue is difficult to explore, when the obvious influence of the complex phase structure formed.

The conditions N440$_2$, N440$_4$, N490$_2$ and N490$_6$ presented lower corrosion potentials and higher corrosion currents than the N390$_2$ and N390$_6$ conditions. Diffraction analysis revealed an increase of the CrN phase diffraction lines intensity for treatments at 440 or 490 ℃ as a result of the CrN precipitates formation and depletion of solid solution Cr in the nitrided layer.

The mean values of corrosion current (I_{corr}), corrosion potential ($E_{I=0}$) and corrosion rate (CR) are shown in Table 3. It can be seen that the lowest corrosion rates were obtained for treatment at 390 ℃. Statistically, the corrosion rates for the conditions S1175 and N390$_2$ are identical. The corrosion rates calculated for the other conditions are, however, higher.

It can also be seen from the results shown in Fig. 6 and Table 3 that a pit nucleation potential (E_{np}) (corresponding to a sudden rise in current, when pits start to form) was only evident for the supersatur-

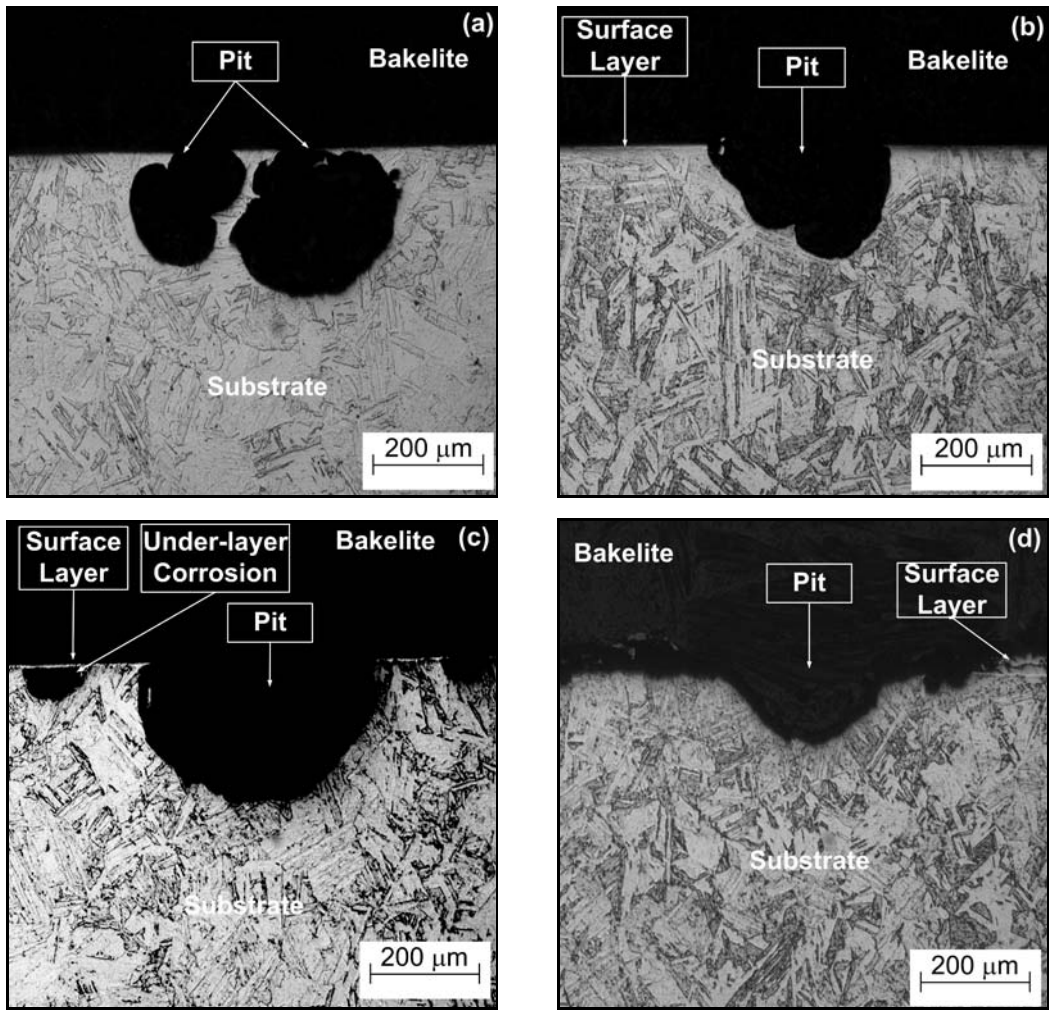

Fig. 7. Micrographs after corrosion tests: a) S1175, b) $N390_2$, c) $N390_6$, d) $N490_6$.

Table 3. Electrochemical parameters for the treatment conditions studied. $E_{I=0}$ – corrosion potential, I_{corr} – corrosion current, E_{np} – pit nucleation potential, CR – corrosion rate

Samples	Parameters			
	$E_{I=0}$, NHE (mV)	I_{corr} (μA cm^{-2})	E_{np} (mV)	CR (mm year^{-1})
S1175	56.4 ± 39.7	0.07 ± 0.02	357.3 ± 51.9	0.80 ± 0.27
$N390_2$	316 ± 39.3	0.08 ± 0.075	–	0.89 ± 0.83
$N490_2$	–84.5 ± 33.7	1.31 ± 0.41	–	14.56 ± 4.66
$N440_2$	12.3 ± 15.9	1.01 ± 0.24	–	12.38 ± 3.09
$N440_4$	–15.0 ± 15.4	0.72 ± 0.32	–	8.00 ± 3.59
$N390_6$	155.8 ± 21.5	0.12 ± 0.04	–	1.38 ± 0.46
$N490_6$	–97.36 ± 42.9	1.17 ± 0.33	–	14.70 ± 1.73

ated samples (S1175). A protection potential was not observed for any of the nitrided conditions studied.

3.4. Surface analysis after corrosion tests

The shape of the pits was characterized based on ASTM G46 [27]. Figures 7a to 7d show the micrographs of transverse cuts of samples solubilized S1175 and nitrided $N390_2$, $N390_6$ and $N490_6$, respectively, using an optical microscopy (OM).

It can be seen from Fig. 7a that the pits produced after cyclic polarization of samples S1175 were of the subsurface type. Figures 7b,c show that the samples nitrided at 390 ℃ have deep, elliptical pits. Corrosion

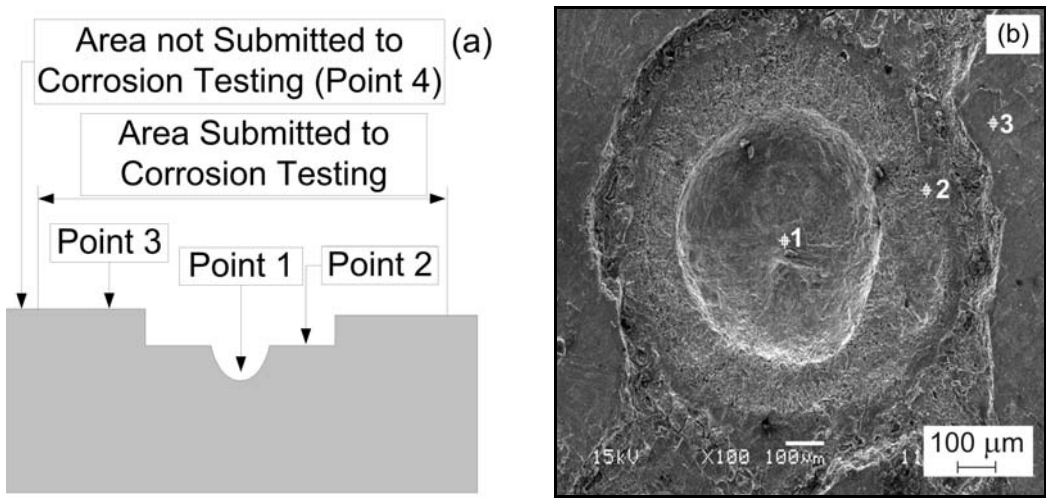

Fig. 8. Locations analysed using EDS after the corrosion tests: a) schematic drawing of the points, b) points in SEM micrograph of an $N440_4$ sample.

was also found under the surface layer in the samples nitrided under the conditions $N390_6$. In this case, during the metallographic preparation, the open part of the pit was removed; this explains the resin under layer (Fig. 7c). It can be seen from Fig. 7d that the pits formed in samples nitrided at 490 ℃ tended to be less deep and wider than those observed for the conditions $N390_2$, $N390_6$ and S1175. Similar results were observed for treatment at 440 ℃. It can also be observed that the surface layer practically disappears after the corrosion tests as a result of the corrosion that it suffers.

Qualitative analyses by a stereomicroscope have shown that the pit density was much higher for samples nitrided at 440 or 490 ℃ than for those nitrided at 390 ℃. According to the ASTM G46 standard [26], whenever very high pit density is verified, corrosion can be considered as generalized.

The presence of pitting indicates that some parts of the surface of the material behave as anodes, inducing localized corrosion. For samples nitrided at 390 ℃, the nobler (uncorroded) regions are larger. As previously mentioned, a higher temperature was found to result in a higher incidence of pitting, e.g., the area where pitting was present increased, although the pits became wider and shallower.

The formation of pits in the samples nitrided at 390 ℃ could be explained by the absence of a homogeneous nitrogen-rich surface layer, according to XRD analysis, the surface layer is multiphase. At higher temperatures, the worse performance is associated with chromium impoverishment around the precipitates of this element.

Few elliptical pits were observed on the surface of samples nitrided at 390 ℃ after corrosion tests, however, in some cases corrosion occurs under the surface layer, which indicates that, in this region, this layer is nobler than the substrate (Fig. 7c), consequently showing better corrosion resistance than the latter. Wide pits were found in samples nitrided at 440 or 490 ℃. Preferential corrosion of the surface layer, causing the exposition of the substrate, was also observed. This corroborates the first statement, e.g., that the surface layer is nobler in samples nitrided at 390 ℃ and less noble in those nitrided at 440 or 490 ℃, suggesting that surface layers formed at low temperatures are nobler than the substrate. This is supported by the cyclic polarization curves, which show that the $E_{I=0}$ is greater for these samples. It appears that samples nitrided at low temperatures had fewer defects (e.g., fewer regions with less noble phases), and thus presented only localized corrosion.

3.5. Energy dispersive spectroscopy analysis

After the corrosion tests the surfaces of samples were analysed using Energy Dispersive Spectroscopy (EDS). Figure 8a shows a schematic illustration and Fig. 8b shows the points on the surface of the analysed samples. Points 1 to 3 lay on the surface submitted to corrosion testing, whereas point 4 corresponds to a non-tested area. Point 1 corresponds to analysis of the bottom of the pit; point 2 to analysis of the region where there was generalized corrosion close to the pits (these regions only appear for nitriding temperatures of 440 and 490 ℃); and point 3 corresponds to a part of the surface which underwent corrosion testing, although no corrosion was apparent (Fig. 8a).

In the Table 4 the results are shown of EDS realized in the points 1, 2, 3, and 4. It can be seen from this table that:

– No nitrogen was observed at point 1 (the region inside the pit). This result was expected, as the depth

Table 4. The results of EDS analysis for different treatment conditions

Condition	Points	Elements		
		N (wt.%)	Cr (wt.%)	Fe (wt.%)
S1175	1	–	18.6 ± 0.7	77.7 ± 1.7
	3	–	14.2 ± 0.3	71.0 ± 0.8
	4	–	14.5 ± 0.4	72.5 ± 0.9
$N390_2$	1	–	14.9 ± 0.3	70.0 ± 0.8
	3	13.6 ± 0.7	12.3 ± 0.3	61.3 ± 0.7
	4	10.9 ± 0.6	13.2 ± 0.3	63.4 ± 0.7
$N390_6$	1	–	15.4 ± 0.3	70.5 ± 0.7
	3	12.6 ± 0.9	14.1 ± 0.3	56.0 ± 0.7
	4	11.6 ± 0.7	15.2 ± 0.4	64.3 ± 0.8
$N440_2$	1	–	14.8 ± 0.3	71.9 ± 0.7
	2	–	34.5 ± 0.4	22.5 ± 0.5
	3	13.7 ± 0.9	18.0 ± 0.3	39.5 ± 0.5
	4	11.3 ± 0.8	12.9 ± 0.3	63.9 ± 0.7
$N440_4$	1	–	15.4 ± 0.3	73.7 ± 0.7
	2	12.3 ± 0.9	25.0 ± 0.3	21.8 ± 0.4
	3	12.4 ± 0.8	13.7 ± 0.3	57.5 ± 0.6
	4	8.2 ± 0.7	13.6 ± 0.3	62.6 ± 0.8
$N490_2$	1	–	15.2 ± 0.3	73.2 ± 0.8
	2	9.1 ± 1.1	18.3 ± 0.3	44.7 ± 0.6
	3	13.0 ± 1.0	12.7 ± 0.3	58.5 ± 0.7
	4	10.5 ± 0.9	13.8 ± 0.3	63.8 ± 0.8
$N490_6$	1	–	14.6 ± 0.3	71.2 ± 0.8
	2	–	18.9 ± 0.3	64.7 ± 0.8
	3	6.5 ± 0.7	13.4 ± 0.3	61.4 ± 0.7
	4	9.6 ± 0.9	14.1 ± 0.3	58.3 ± 0.8

of the pit is greater than the depth of the nitrided surface layer;

– In region 2, the amount of chromium was greater than that found in the other regions submitted to corrosion testing. In some cases the amount of chromium found was as high as 34 % ($N440_2$). A reduction in the amount of iron can also be observed in this region. This fact is associated to the selective corrosion of iron and consequent chromium enrichment in this region;

– Comparing the amounts of chromium from points 4 (the region not submitted to corrosion testing) and 3 (the region submitted to corrosion testing, without apparent corrosion) shows the same values for both points. Due to the presence of selective corrosion, two regions were formed on the surface exposed to corroding environment: the first, the anode, formed by the pit, and the second, the cathode, formed by region 3. Consequently, no corrosion was apparent in this region.

4. Conclusion

Based on the experimental results, the following conclusions can be drawn from the present investigation:

– Higher core hardness is favoured by low treatment temperature and long treatment time, whereas high treatment temperature (490 ℃) favours the overageing process. For the conditions $N440_4$, the overageing process was found to have already begun.

– For the studied treatment conditions, the growth of the surface layer (thickness) is favoured by longer treatment times and higher temperatures. The maximum hardness of the surface layer was achieved in the treatment where the highest temperature and the longest time were used.

– The supersaturated conditions (S1175) produced a tendency to passivation during the E_{corr}-versus-time test. The nitriding conditions $N390_2$ and $N390_6$ yielded nobler potentials than the supersaturated conditions. However, the films formed were not stable and caused large changes in potential during the tests, due to the absence of closed and homogeneous nitrogen-rich layer.

– Based on the results of cyclic polarization tests, the nitriding conditions $N390_2$ and $N390_6$ had nobler corrosion potentials than the supersaturated conditions S1175; notwithstanding that there was a very narrow passive region under these conditions.

– The conditions $N440_2$, $N490_2$ and $N490_6$ produced lower corrosion potentials ($E_{I=0}$) than the supersaturated conditions S1175; however, under these conditions the corrosion tends to be generalized. This can be associated to CrN phase precipitation and consequently solid solution Cr impoverishment within the surface.

– The supersaturated sample (S1175) showed subsurface pitting. The samples nitrided at 390 ℃ were found to have deep, elliptical pits. The conditions $N390_6$ resulted in corrosion beneath the surface layer indicate that the surface layer is nobler than the matrix. The pits in samples nitrided at 440 or 490 ℃ tend to be wider and shallower.

Acknowledgements

The authors would like to thank the Postgraduate Program in Mechanics and Materials Engineering at UTFPR; the CNPq for financial support; the Mineral and Rock Laboratory (LAMIR) at UFPR; the Center for Electronic Microscopy (CME at UFPR); the Santa Catarina Educational Society (SOCIESC); and SpectroScan Tecnologia de Materials Ltda.

References

[1] DONG, H.—ESFANDIARI, M.—LI, X. Y.: Surf. & Coat. Technol., *202*, 2008, p. 2969. doi:10.1016/j.surfcoat.2007.10.036

[2] LI, G. J.—WANG, J.—LI, C.—PENG, Q.—GAO, J.—SHEN, B. L.: Nucl. Instr. Meth. B. (article in press).

[3] COHEN, A.—BOAS, M.—ROSEN, A.: Thin Solid Films, *141*, 1986, p. 53. doi:10.1016/0040-6090(86)90318-4

[4] ÇELIK, A.—ARSLAN, Y.—YETIM, A. F.—EFEOGLU, I.: Kovove Mater., *45*, 2007, p. 35.

[5] BLAWERT, C.—MORDIKE, B. L.—COLLINS, G. A.—SHORT, K. T.—TENDYS, J.: Surf. Coat. Technol., *103–104*, 1998, p. 240. doi:10.1016/S0257-8972(98)00402-2

[6] LI, C. X.—BELL, T.: Corrosion Science, *46*, 2004, p. 1527. doi:10.1016/j.corsci.2003.09.015

[7] ODDERSHEDE, J.—CHRISTIANSEN, T. L.—STAHL, K.—SOMERS, M. A. J.: J. Mater. Sci., *43*, 2008, p. 5358. doi:10.1007/s10853-008-2791-y

[8] MENTHE, E.—BULAK, A.—OLFE, J.—ZIMMERMANN, A.—RIE, K. T.: Surf. Coat. Technol., *133–1134*, 2000, p. 259.

[9] MARINHO, R. R.—PIANA, L. A.—STROHAECKER, T. R.: COTEQ – 6a Conferęncia Sobre Tecnologia de Equipamentos, 6th COTEQ, Salvador 2002 (on CD rom).

[10] MÄNDL, S.—FRITZSCHE, B.—MANOVA, D.—HIRSCH, D.—NEUMANN, H.—RICHTER, E.—RAUSCHENBACH, B.: Surface & Coatings Technology, *195*, 2005, p. 258.

[11] LEI, M. K.—ZHANG, Z. L.—ZHU, J. X. M.: Mater. Sci. Lett., *18*, 1999, p. 1537. doi:10.1023/A:1006658820963

[12] ESFANDIARI, M.—DONG, H.: Surface Engineering, *22*, 2006, p. 86. doi:10.1179/174329406X98368

[13] MANOVA, D.—THORWARTH, G.—MÄNDL, S.—NEUMANN, H.—STRITZKER, B.—RAUSCHENBACH, B.: Nucl. Instr. and Meth. B, *242*, 2006, p. 285. doi:10.1016/j.nimb.2005.08.059

[14] FRANDSEN, R. B.—CHRISTIANSEN, T.—SOMERS, M. A. J.: Surf. Coat. Technol., *200*, 2006, p. 5160. doi:10.1016/j.surfcoat.2005.04.038

[15] BORGES, P. C.—MARTINELLI, A. E.—FRANCO, C. V.: Materials Corrosion, *55*, 2004, p. 594. doi:10.1002/maco.200303784

[16] KUMAR, S.—BALDWIN, M. J.—FEWELL, M. P.—HAYDON, S. C.—SHORT, K. T.—COLLINS, G. A.—TENDYS, J.: Surf. Coat. Technol., *123*, 2000, p. 29. doi:10.1016/S0257-8972(99)00393-X

[17] PRIEST, J. M.—BALDWIN, M. J.—FEWELL, M. P.: Surf. Coat. Technol., *145*, 2001, p. 152. doi:10.1016/S0257-8972(01)01311-1

[18] BAJGUIRANI, H. R. H.: Mat. Science Engin., *A338*, 2002, p. 142.

[19] HABIBI, H. R.: Materials Letters, *59*, 2005, p. 1824. doi:10.1016/j.matlet.2004.09.058

[20] PORTER, D. A.—EASTERLING, K. E.: Phase Transformations in Metals and Alloys. London, Van Nostrand Reinhold 1981.

[21] OLIVEIRA, S. D.: Tratamento Duplo de Envelhecimento e Nitretação por Plasma Pulsado em um Aço Ferramenta Endurecível por Precipitação. Dissertação de Mestrado, Universidade de São Paulo 1999.

[22] JEONG, B. Y.—KIM, M. H.: Surf. Coat. Technol., *137*, 2001, p. 249. doi:10.1016/S0257-8972(00)01095-1

[23] SUN, Y.—LI, X. Y.—BELL, T.: J. Mater. Sci., *34*, 1999, p. 4793. doi:10.1023/A:1004647423860

[24] YETIM, A. F.—YILDIZ, F.—ALSARAN, A.—ÇELIK, A.: Kovove Mater., *46*, 2008, p. 105.

[25] ÁLVARO, R. V.—BENEITEZ, A. P.—VÁZQUEZ, J. R.—CALLEJAS, R. L.—BAROCIO, S. R.—CABRERA, O. G. G.—CABRERA, A. M.—EQUILUZ, R. P.—CASTRO, A. E. M.: Vacuum, *81*, 2007, p. 1434.

[26] ASTM G5. Standard Reference Test Method for Making Potentiostatic and Potentiodynamic Anodic Polarization Measurement, 1994.

[27] ASTM G46. Standard Guide for Examination and Evaluation of Pitting Corrosion, 1994.